



Published in final edited form as:

Lab Invest. 2020 December ; 100(12): 1517–1531. doi:10.1038/s41374-020-0458-8.

CD38 in cancer-associated fibroblasts promotes pro-tumoral activity

Bar Ben Baruch¹, Einav Mantsur¹, Janusz Franco-Barraza², Eran Blacher^{1,*}, Edna Cukierman^{2,†}, Reuven Stein^{1,†}

¹Department of Neurobiology, School of Neurobiology, Biochemistry and Biophysics, George S. Wise Faculty of Life Sciences, Tel Aviv University, Israel.

²Cancer Biology, the Marvin & Concetta Greenberg Pancreatic Cancer Institute, Fox Chase Cancer Center, Philadelphia, PA, United States.

Abstract

Primary and metastatic melanoma progression are supported by a local microenvironment comprising, *inter alia*, of cancer-associated fibroblasts (CAFs). We previously reported in orthotopic/syngeneic mouse models that the stromal ectoenzyme CD38 participates in melanoma growth and metastasis. The results presented here suggest that CD38 is a novel regulator of CAFs' pro-tumorigenic functions. Orthotopic co-implantation of CD38 deficient fibroblasts and B16F10 melanoma cells limited tumor size, compared to CD38 expressing fibroblasts. Intrinsically, CAF-CD38 promoted migration of primary fibroblasts toward melanoma cells. Further, *in vitro* paracrine effects of CAF-CD38 fostered tumor cell migration and invasion as well as endothelial cell tube formation. Mechanistically, we report that CAF-CD38 drives the protein expression of an angiogenic/pro-metastatic signature, which includes VEGF-A, FGF-2, CXCL-12, MMP-9 and HGF. Data suggest that CAF-CD38 fosters tumorigenesis by enabling the production of pro-tumoral factors that promote cell invasion, migration and angiogenesis.

Introduction

Melanoma is considered the deadliest skin cancer [1]. Like many other solid cancers, the melanoma tumor mass is comprised of cancer (i.e., melanocytes) and tumor microenvironment (TME) cells. The main melanoma TME cells include a collection of immune, endothelial and cancer-associated fibroblastic (CAFs) [2]. Physiologically, fibroblasts secrete and maintain the interstitial extracellular matrix (ECM), which regulates the local homeostatic equilibrium[3]. Fibroblasts can be activated and alter the ECM as well

Users may view, print, copy, and download text and data-mine the content in such documents, for the purposes of academic research, subject always to the full Conditions of use:http://www.nature.com/authors/editorial_policies/license.html#terms

[†]Corresponding authors: Reuven Stein, Department of Neurobiology, School of Neurobiology, Biochemistry and Biophysics, George S. Wise Faculty of Life Sciences, Tel Aviv University, 69978 Ramat Aviv, Israel. Phone: (972) 3 640 8608; Fax: (972) 3 640 7643; reuven@tauex.tau.ac.il, Edna Cukierman, Cancer Biology, the Marvin & Concetta Greenberg Pancreatic Cancer Institute, Fox Chase Cancer Center, Philadelphia, PA, United States. edna.cukierman@fccc.edu.

*Current address: Department of Neurology & Neurological Sciences, Stanford School of Medicine, Stanford, CA, USA

sure/Conflict of Interest

The authors declare no conflict of interest.

as their secretomes during activation, such as in wound healing. Activated fibroblasts are either eliminated or able to regain homeostatic features upon wound resolution [4]. However, during chronic inflammatory and/or fibrotic conditions, like in cancers such as melanoma [5], activated fibroblasts (i.e., CAFs) persist and continuously support tumor growth, invasion and angiogenesis [6]. Of note, we previously showed that discrete CAF traits predict overall survival [7–9]. In this study, we investigate the functional roles of a CAF-relevant protein, CD38, in melanoma [10].

CD38 is a nicotinamide adenine dinucleotide (NAD⁺) glycohydrolase and adenosine diphosphate (ADP)-ribosyl cyclase known to functionally participate in chronic inflammatory conditions such as asthma, diabetes, obesity, heart disease, aging, and cancer [11–14]. We have previously reported that targeting stromal CD38 in melanoma increases cell death in the tumor mass and reduces CAF density and numbers of blood vessel [10]. Further, CD38 knockout (*Cd38*^{-/-}), or its pharmacological inhibition, limits both glioma [15, 16] and melanoma progressions, including metastasis [10]. Since CAFs are known to promote tumor progression and angiogenesis in melanoma [5], we hypothesized that CAF-CD38 exerts a key role in these functions. These findings show that CD38-expressing CAFs promote tumor cell migration and invasion as well as blood vessel formation, *in vitro*. We report using an *in vivo* co-implantation system, that melanoma progression is facilitated by fibroblastic-CD38 and suggest a role for CAF-CD38 in enabling the expression of key metastatic and angiogenic factors like VEGF-A, FGF-2, CXCL-12, MMP-9 and HGF.

Materials and Methods

Reagents

Unless otherwise stated, reagents were purchased from Sigma-Aldrich (St. Louis, MO,) and cell culture media from Invitrogen Life Technologies (Paisley, UK).

Mice

C57BL/6J *Cd38*^{-/-} mice were generated and described previously [17]. WT C57BL/6J mice were purchased from Envigo [Jerusalem Israel (bl-6r252)]. Animals were bred and maintained at the Tel-Aviv University (TAU) animal facility under defined-flora and pathogen-free conditions. All studies were performed according to protocols approved by the Animal Care and Use Committee of TAU. To prevent animal suffering, tumor bearing mice were evaluated 3 times per week focusing on signs of sickness or distress, which included tumor size as well as weight loss according to institutional guidelines.

Cell lines

B16-F10 melanoma cells (RRID:CVCL_0159) stably expressing mCherry (herein B16F10), were maintained as previously described. [10] Murine skin tumor associated fibroblasts, MTAF1.1, were referred to as MTAF throughout the text. MTAF cells are *bona fide* dermal CAFs, isolated from a two-stage carcinogenic squamous cell carcinoma model and immortalized by natural catastrophe induced by *in vitro* cultivation [18]. MTAFs were used as these CAFs were shown to produce *in vivo* like ECMs, which assist the cells to retain *in vivo* like phenotypes and functions throughout numerous passages (just like any other

immortalized CAF cell line). [19] Immortalized mouse endothelial cells, CLU510 or MCEC (herein MECs) were obtained from Cedarlane (Burlington, Ontario). PDSC5 cells, HPV16-positive murine squamous cell carcinoma cell line [20], were obtained from Prof. Neta Erez (TAU). MTAF, MECs and PDSC5 were maintained in DMEM, supplemented with 10% fetal calf serum (FCS), 1% P/S. All cells were routinely tested for Mycoplasma using the EZ-PCR Mycoplasma Test Kit (Biological industries, Beit-Haemek, Israel).

Preparation of mouse primary dermal fibroblasts

Skin tissue samples were surgically-removed from naïve wild type (WT) and *Cd38*^{-/-} newborn mice and incubated in 0.25% trypsin at 4°C for 16 h, followed by additional incubation with fresh 0.25% trypsin (15 min; 37°C). Dermis was isolated, chopped, dispersed into a single-cell suspension and seeded into 6-well plates. Low passages (3–5) of the cultures were used for the experiments.

Sorting MTAF cells into MTAF CD38^{high} and MTAF CD38^{low} cell populations

MTAF cells (5×10^5) were incubated with anti-mouse CD16/CD32 mAb (clone 93, 1:50) (#14-0161-81, eBioscience™; San Diego, CA, USA) during 20 min at 4°C for Fc blockade, then with anti-mouse CD38 mAb (clone 90, 1:166) (#12-0381-81, eBioscience™; San Diego, CA, USA) for additional 45 min. Cells were washed using cold PBS, filtered, and sorted by BD FACSAria III (BD Biosciences, NJ) into CD38^{high} and CD38^{low} populations. The sorted cells were expanded for 4–5 passages, followed by validation of CD38 expression levels using the CytoFLEX flow cytometer (Beckman Coulter, CA, USA).

CD38 enzymatic activity

CD38 enzyme activity was measured using the substrate 1, *N*⁶-etheno-nicotinamide adenine dinucleotide⁺ (ε-NAD⁺) as described [16].

Immunoblotting

Primary B16F10 melanoma tumors were established in C57BL/6J WT or *Cd38*^{-/-} mice (syngeneic mouse model). Briefly, B16F10 cells (50,000 / 100 μl) were subcutaneously injected into the right flank of WT or *Cd38*^{-/-} mice as described [10]. Tumors were excised from WT and *Cd38*^{-/-} B16F10 melanoma-bearing mice at 28 days post-injection and homogenized in lysis buffer [50 mM Tris-HCl (pH 7.6), 20 mM MgCl₂, 200 mM NaCl, 0.5% NP40, 1 mM DTT, and 1 mM antiproteases]. Samples containing 50 μg of protein were resolved in 12% SDS-PAGE gels and electroblotted onto nitrocellulose membranes. Blotted membranes were blocked with Tris-buffered saline/Tween-20 (10 mM Tris base, 150 mM NaCl, 0.05% Tween-20) containing 5% fat-free milk for 1 h, followed by incubation with rabbit anti-αSMA pAb (Abcam Ab5694, 1:500), rabbit anti-GAPDH mAb (Cell signaling #2118, 1:1000), or mouse anti-β-tubulin mAb (Sigma #T4026, 1:2500) at 4°C, overnight. Membranes were then incubated with goat anti-rabbit IgG peroxidase conjugate (1:10,000; Jackson ImmunoResearch Laboratories). Blots were processed using Luminata Crescendo Western HRP chemiluminescence Substrate (Millipore, MA, USA) and visualized by the Amersham Imager 600 (GE Healthcare Life Sciences). Signal of αSMA was normalized to β-tubulin and quantified using ImageJ.

B16F10 melanoma/primary fibroblasts co-implantation

B16F10 melanoma cells (5×10^4) mixed with 1.5×10^5 primary WT or *Cd38*^{-/-} fibroblasts (ratio 1:3 in 100 μ l of cells suspension) were subcutaneously injected into the right flanks of WT or *Cd38*^{-/-} mice. Since the B16 cells were originally harvested from female C57BL mice, we used female mice in an attempt to match the host sex and thus obtain a syngeneic model. Tumor size was monitored daily using a caliper, and ellipsoid volume was calculated by $\pi/6 \times (L \times W \times H)$. Endpoint was determined when one of the tumor's dimensions reached 1.5 cm. Survival duration of the mice was recorded, visualized by Kaplan-Meier plots, and analyzed via a log-rank test.

Conditioned media preparation

Conditioned media were prepared from co-cultures of B16F10 cells and primary fibroblasts. 1.5×10^6 WT or *Cd38*^{-/-} primary fibroblasts were plated, with or without 5×10^5 B16F10 cells, in DMEM supplemented with 10% FCS and 1% P/S. Separately, 5×10^5 B16F10 cells were plated using the same medium. Cells were allowed to attach for 5 h, followed by medium replacement using DMEM, supplemented with 2% FCS and 1% P/S and continue culturing at 37°C. After 72 h, the medium was collected, cleared of cell debris by centrifugation, and supernatant was filtered through 0.22 μ m filter (Sartorius, Göttingen, Germany) to obtain condition media (CM). Note that CM was aliquoted and stored frozen at -80°C until used. Aliquots were thawed in a 37°C water bath prior usage for each experiment.

MTAF-derived 3D cultures and CM preparations

As mentioned above, MTAF cells are CAFs and as such these cells retain known *in vivo*-like desmoplastic characteristics while producing ECM (i.e., in 3D) [18]. 3D matrix producing MTAF cultures were prepared as described [21]. Briefly, 24-well plates were incubated with 0.2% gelatin solution for 1 h at 37°C, followed by 30 min fixation with 1% glutaraldehyde, and additional 30 min incubation with 1M ethanolamine at room temperature. Wells were washed and plated with 3×10^5 MTAF CD38^{high} or MTAF CD38^{low} cells/well in 0.5 ml of DMEM supplemented with 10% FCS and 1% Penicillin-Streptomycin. Cells were cultured at 37°C for 5 days and supplemented daily with freshly-prepared ascorbic acid (50 μ g/ml). Immunofluorescence quality control experiments to assure ECM traits and thickness were conducted as published [21]. For CM, unextracted MTAF cultures, at the end of matrix production, were washed with PBS followed by 48 h incubation in serum-free DMEM (SFM). After that, CM (herein CD38^{high} 3D CM and CD38^{low} 3D CM, respectively) were collected, filtered through 0.22 μ m filters and stored at -80°C as before.

MTAF CD38^{high} and MTAF CD38^{low} 2D cultures

MTAF CD38^{high} and MTAF CD38^{low} cells (5×10^4) were plated in 25 cm² flasks and cultured for 18 h, as described above. Growth medium was replaced with either B16F10 CM or SFM for additional 48 h, followed by cell harvesting for RNA extraction. B16F10 CM was prepared from 1.5×10^6 B16F10 cells seeded in 25 cm² flasks and cultured for 18 h. Cells were washed with PBS, supplemented with SFM and incubated for 24 h, prior to CM collection and filtering through 0.22 μ m filters.

Transwell Migration

WT and *Cd38*^{-/-} primary fibroblasts (5×10^5), B16F10 cells (2×10^5), or PDSC5 cells (2×10^5) were plated on the upper side of collagen-coated 24-well (i.e., transwell) inserts (8 μ m pore size), in 100 μ l DMEM containing 0.1% BSA. Assorted 10^5 cells (i.e., B16F10 or CD38^{high} vs. CD38^{low} MTAFs) were plated onto the lower chamber. Alternatively, CM collected from primary fibroblasts, co-cultures of B16F10 cells and primary fibroblasts or from 3D cultures of CD38^{high} vs CD38^{low} CAFs (650 μ l) was deposited into the lower chamber. After 24 h, inserts' upper sides were gently scraped to remove non-migrating cells and lower sides were fixed with 4% paraformaldehyde for 30 minutes, washed twice with PBS and stained with 1 μ g/ml Hoechst 33342 (Invitrogen Life Technologies, Paisley, UK). Controls (not shown) included quantification of cell growth to assure differences recorded were due to changes in cell migration. Images corresponding to 8–10 fields per insert were captured using EVOS® FL fluorescence microscope ($\times 10$ magnification), and nuclei numbers were gauged in ImageJ.

Wound healing assay

Wound healing assay was performed as described [16]. Briefly, 1.5×10^6 B16F10 cells/well were cultured in 6-well plate for 24 h. Medium was replaced with PBS and three areas were scratched, producing three gaps of similar widths, using a blue pipet tip. Gentle washes with PBS were used to remove floating cells, PBS was replaced with CM, scratched areas were photographed, and cells were incubated for an additional 24 h at 37°C prior to acquiring images of the scratched areas for a second time. Bright-field images were captured using EVOS® FL microscope ($\times 4$ magnification) and the gap width was measured and quantified using ImageJ.

Matrix and transendothelial Invasion

Matrix invasion- Cultrex (i.e., Matrigel) basement membrane substrate (50 μ l) (Trevigen, Gaithersburg, MD) (5 mg/ml) was added on top of collagen-coated 8 μ m transwell inserts and allowed to solidify for 1 h at 37°C. B16F10 or PDSC5; 5×10^5 cells per 100 μ l DMEM containing 0.1% BSA, were seeded on top of the solidified matrix.

Trans-endothelial invasion- 4×10^5 MECs, cultured in their own growth medium, were seeded on the upper side of 0.2% gelatin-coated transwell and incubated for 24 h at 37°C. B16F10, 5×10^5 cells per 100 μ l DMEM containing 0.1% BSA, were seeded on top of the MECs monolayer. In both assays, 650 μ l of the tested CM were added to the lower chamber. After 24 h, the inserts were removed, and their upper side was scraped with cotton swabs. Invaded cells, on the lower side of the insert, were fixed using 4% paraformaldehyde for 30 minutes, washed twice with PBS and counterstained with Hoechst 33342. Eight to 10 fields per insert were captured using EVOS® FL fluorescence microscope ($\times 10$ magnification), and numbers of nuclei in each field were gauged with ImageJ.

Tube formation assay

Tube formation assay was performed as described [22] with only a few modifications. Briefly, 24-well culture plates were pre-coated with 250 μ l/well of 10 mg/ml Cultrex that was allowed to solidify for 1 h at 37°C. MECs (10^5 cells) were suspended in 50 μ l growth

medium and mixed with 450 μ l of assorted CM. Cells were seeded onto the Cultrex-coated wells. Following 8–10 h incubation, 7 bright-field images were captured per well using EVOS® FL microscope equipped with a 10X objective. Images were analyzed by Angiogenesis Analyzer plugin in ImageJ.

Angiogenesis profiler array

MTAF CD38^{high} and MTAF CD38^{low} cells were grown in a 24-well plate (12 wells for each cell type), under 3D matrix-producing conditions, and CM was collected as described above. CM from 12 wells were collected and pooled together. After CM collection, cell lysate buffer, obtained from Mouse Angiogenesis Profiler Array Kit (ARY015, R&D Systems, Minneapolis, MN), was added to the wells, and lysates were also pooled together. As quality control we vetted that the CM collected effectively induced CD38-dependent tube formation (not shown). Expression of angiogenesis-related proteins, in the cell lysates, was profiled using the Mouse Angiogenesis Profiler Array Kit according to manufacturer's protocol. The arrays were imaged with Amersham Imager 600 (GE Healthcare Life Sciences). Quantification of signal intensity was performed with ImageJ. Results shown are from two independent experiments. To verify equal amounts of assessed MTAF CD38^{high} and MTAF CD38^{low} proteins, cell lysate GAPDH levels were measured by immunoblotting as described above.

RNA extraction and Quantitative real-time PCR (qRT-PCR)

Reagents were purchased from Thermo Fisher Scientific. RNA was purified from MTAF CD38^{high} and MTAF CD38^{low} in 2D and 3D cultures (as above), pooling four wells per experimental sample, using Trizol® reagent and 1.5 μ g were reverse transcribed (high-capacity cDNA RT kit). Using 10 ng cDNA as a template, qRT-PCR was performed using Absolute Blue SYBR Green PCR mix. The following listed primers were employed:

Gapdh F: CATGGCCTTCCGTGTTCCCTA, R: ATGCCTGCTTACCACCTTCT

Cxcl12 F: CAGAGCCAACGTCAAGCATC, R: TTAATTTCTGGGTCAATGCACAC

Hgf F: AACAGGGGCTTTACGTTCACT, R: CGTCCCTTTATAGCTGCCTCC

Fgf2 F: GCGACCCACACGTCAAACCTA, R: CCGTCCATCTTCCTTCATAGC

Mmp9 F: GCAGAGGCATACTTGTACCG, R: TGATGTTATGATGGTCCCCTTG

Vegfa F: TAACGATGAAGCCCTGGAGT, R: GCCTTGGCTTGTCACATTTT.

Expression values were normalized to *GAPDH*, and RQ (2^{-C_t}) was calculated.

Statistical analysis

Two-way ANOVA with repeated measures followed by Tukey post-hoc tests were used to compare tumor volume in WT and *Cd38*^{-/-} mice, co-injected with WT or *Cd38*^{-/-} fibroblasts. The data was log transformed to reach normal distribution. Survival was analyzed by a log-rank test. Other experiments were analyzed, by Two-way ANOVA,

followed by Bonferroni post-hoc test, or by an unpaired two-tailed Student's *t* test; (* $p < 0.05$, ** $p < 0.01$, *** $p < 0.001$).

Results

Fibroblastic CD38 expression promotes melanoma tumorigenesis

Using the B16F10 melanoma syngeneic mouse model, we previously reported that stromal loss of CD38 decreased both CAF numbers (i.e., noting α -SMA positive stromal cells) and tumor growth, while increasing the lifespan of melanoma-bearing C57BL/6J mice [10]. To further validate these findings, we again evaluated expression levels of α -SMA, this time in tumor masses in which proteins were resolved via SDS-PAGE and detected via immunoblotting. As expected, α -SMA levels were significantly reduced in tumors implanted in *Cd38*^{-/-} mice, compared to WT host controls (Fig. 1a, b), suggesting a diminished number in activated fibroblastic cells, as before [10]. Furthermore, the enzymatic CD38 activity, in fibroblasts, was verified *in vitro* using primary dermal fibroblasts harvested from WT vs. *Cd38*^{-/-} mice (Fig. 1c). The central premise of this study is that CAF-CD38 would foster tumorigenesis. To test this hypothesis, we co-injected B16F10 and primary dermal WT or *Cd38*^{-/-} fibroblasts into WT or *Cd38*^{-/-} recipient mice. As controls, WT or *Cd38*^{-/-} mice were injected with B16F10 cells alone (as before [10]). As expected, *Cd38*^{-/-} mice injected with B16F10 cells developed significantly smaller tumors than in WT mice [Fig. 1d; 2.6 fold ($p = 0.02$) reduction at day 24 post-injection]. Of note, when B16F10 were co-injected with WT fibroblasts, tumors grew significantly larger, compared to tumor cells alone, regardless of the CD38 status in the host/recipient mice [Fig. 1d; 1.7-fold ($p = 0.02$) and 4-fold ($p < 0.001$) at day 24 post-injection, in WT and *Cd38*^{-/-} mice respectively]. Interestingly, co-injections of B16F10 and *Cd38*^{-/-} fibroblasts, using WT mice as hosts, rendered significantly smaller tumors compared to B16F10 cells alone [Fig. 1d; 2.1-fold ($p = 0.03$) at day 24 post-injection]. Moreover, *Cd38*^{-/-} mice co-injected with B16F10 and *Cd38*^{-/-} fibroblasts or with B16F10 cells alone, rendered the smallest tumor volumes, with no significant differences between the two (Fig. 1d). In line with these results, Kaplan Meier curves (Fig. 1e) revealed that loss of fibroblastic CD38 suffices to prolong survival times while fibroblasts expressing CD38 significantly shortened survival. Taken together, results suggest a pro-tumor role for fibroblastic CD38.

CD38 promotes fibroblastic cell migration in the direction of tumor cells

To further query why we previously observed a decrease in CAF accumulation in *Cd38*^{-/-} mice [10], we tested the hypothesis that *Cd38*^{-/-} fibroblasts are chemotactically impaired and thus insensitive to melanoma secreted factors. To test this, we used the Boyden chamber assay and measured the 24 h migratory capacity of WT vs. *Cd38*^{-/-} fibroblasts in response to B16F10 seeded in the bottom chamber. Results showed about 2.5 fold ($p < 0.001$) reduction in migration of *Cd38*^{-/-} fibroblasts towards B16F10, compared to WT fibroblasts (Fig. 2a, b). These results suggested a role for CD38 in regulating fibroblastic migration in response to melanoma-produced chemoattractants.

CAFs enhance melanoma invasive behavior and support angiogenesis in a CD38-dependent manner

Given that CAFs are known to support melanoma cells' migration and invasion [5, 23], we examined the role of fibroblastic CD38 in these tumor cell functions. The migration of B16F10 cells was evaluated using wound healing (i.e., scratch) assays [24], in which the effect of assorted fibroblastic conditioned media (CM) on the migratory capability of B16F10 cells was assessed. CM collected either from fibroblastic monocultures or from co-cultures of fibroblasts and B16F10 cells, were compared to CM from B16F10 alone. Treating melanoma cells with CM obtained from WT fibroblasts resulted in substantial closure of the wounded gap, at 24 h. In comparison, an important delay in gap resolution was observed if tumor cells were treated with CM obtained either from fibroblastic *Cd38*^{-/-} alone or co-cultured with B16F10 cells (Fig. 2c, d). Cell growth ratios (not shown) could not account for the observed differences. Taken together, results suggest that fibroblastic CD38 stimulates melanoma cell motility.

CAFs have been shown to promote cancer cell invasion (i.e., cell intravasation) [25]. Since we reported that stromal CD38 promotes melanoma metastases [10], and observed that CM from CD38-null fibroblasts reduces migration of melanoma cells *in vitro* (Fig. 2), we next examined the effect that fibroblasts expressing CD38 impart on cancer cell invasion. Using the basement membrane coated (Cultrex) Boyden chamber assay, we observed that CM from WT fibroblasts significantly increased melanoma cell invasion, compared to control (i.e., CM obtained from B16F10) or to CM obtained from *Cd38*^{-/-} fibroblasts (2 or 2.6 fold vs control or *Cd38*^{-/-} fibroblasts CM respectively, $p < 0.001$) (Fig. 3a and 3b). Importantly, CM obtained from co-cultures that included *Cd38*^{-/-} fibroblasts, significantly impaired tumor cell invasion, compared to co-cultures with WT fibroblasts (1.8 times less, $p < 0.05$) (Fig. 3a, b). Results suggested that CM collected from WT fibroblasts could contain pro-invasive factors (or lack inhibitory ones).

We also compared the fibroblastic CM effects (i.e., WT vs *Cd38*^{-/-}) imparted on melanoma cells during trans-endothelial invasion. For this, we seeded mCherry-labeled B16F10 cells onto monolayers of murine endothelial cells (MECs). Results shown in Figures 3c and 3d, demonstrate that CM obtained from WT fibroblasts, but not from *Cd38*^{-/-} cells, increased B16F10 trans-endothelial (i.e., MEC) invasion compared to CM from B16F10 (controls) (2.2 fold vs control, $p < 0.001$). Furthermore it also increased B16F10 trans-endothelial invasion, compared to CM obtained from *Cd38*^{-/-} cells (1.8 fold vs *Cd38*^{-/-} cells, $p < 0.01$).

Treatment with CM collected from co-cultures again resembled the use of fibroblastic CM (Fig. 3c, d) (4.2 fold vs control, $p < 0.001$). Collectively, these results also support the notion that intact fibroblastic cells, but not CD38 deficient ones, could secrete factors that support migration and invasion of B16F10 melanoma cells.

It is well accepted that CAFs support angiogenesis [26]. Since we previously reported that loss of stromal CD38 limits blood vessel density in melanoma [10], we hypothesized that fibroblastic CD38 plays a role in endothelial angiogenic tube formation. For this, the extent of MEC capillary-like network formation (Fig. 4a), was assessed gauging total vessel length

(Fig. 4b), number of junctions (Fig. 4c), and amount of meshes built (Fig. 4d). Results showed that CM collected from WT fibroblasts, either from mono or co-cultures with B16F10 cells, prompted an increase in MEC tube formation when compared to effects imparted using CM from *Cd38*^{-/-} fibroblasts mono or co-cultures with B16F10 cells. It is important to note that this increase included all measured aspects of tube formation (Figs. 4b–d) [e.g., total length; 1.5 and 1.7 fold increase compared to *Cd38*^{-/-} fibroblasts mono or co-cultures with B16F10 cells respectively ($p < 0.001$) (Fig. 4b)]. These results support the notion that endothelial tube formation modulating factors secreted by fibroblasts is CD38 dependent.

To further strengthen our findings, we query whether the observed CD38 regulated pro-tumorigenic functions could be detected using additional fibroblastic cells. Murine tumor associated fibroblasts (MTAFs), or murine CAFs, were obtained from a mouse squamous cell carcinoma model [18] and sorted into CD38^{high} and CD38^{low} expressing sub-populations (supplementary Fig S1a–c). CD38 enzymatic activity assays were performed to validate the correlation between levels of CD38 expression and CD38 function in the sorted MTAF CD38^{high} and CD38^{low} cells (supplementary Fig. S1d).

Importantly, CAFs generated extracellular matrices (ECMs) are known to participate in the regulation of metastasis [9, 23, 27]. Furthermore, by culturing MTAFs within self-generated ECMs, in 3D conditions, we have previously reported relevant pathophysiological traits for these murine CAFs and their cell-derived ECMs, similar to desmoplastic features seen *in vivo* [18]. Hence, we examined effects in B16F10 migration and invasion (as before), only this time CM was collected from ECM producing (i.e., 3D cultures) MTAF CD38^{high} vs. MTAF CD38^{low}. In addition, B16F10 migration was examined when MTAF CD38^{high} vs. MTAF CD38^{low} were plated in the bottom chamber. Just as before, migration and invasion of B16F10 cells was limited by CD38 deficient fibroblasts. Accordingly, when treated with CM obtained from MTAF CD38^{high} vs. MTAF CD38^{low} 3D cultures, we observed 1.3 fold increase; CD38^{high} vs CD38^{low} $p < 0.05$, in B16F10 migration (Fig. 5a–b). Similarly, the effect of MTAF CD38^{high} plated on the bottom chamber, on B16F10 migration was 3.2 fold higher ($p < 0.001$) than that of MTAF CD38^{low} (Fig. 5c–d). Lastly, the effect of CM obtained from MTAF CD38^{high} 3D cultures was 4.8 fold higher ($p < 0.001$) than that of CM obtained from MTAF CD38^{low} 3D cultures on B16F10 invasion (Fig. 5e–f). The robustness of our 3D cultured results was tested in an additional skin cancer cell line, PDSC5 [20]. Effects of CM collected from MTAF CD38^{low} vs. MTAF CD38^{high} 3D cultures were comparable to those observed in B16F10 cells (supplementary Fig. S2a–d). Furthermore, the ability of MECs to form tubes was also significantly lower in MECs treated with MTAF CD38^{low} 3D CM compared to MTAF CD38^{high} 3D CM [Fig. 5g–j; 2, 2.14 and 2.7 fold CD38^{high} vs CD38^{low} ($p < 0.001$) total vessel length, number of junctions and amount of meshes]. Collectively, these results suggest a pro-tumoral function for CM secreted by CD38 expressing CAFs and imply a role for CAF-generated ECMs in regulating CAF collected CM.

Angiogenesis-related proteins are regulated in CAFs via CD38

In an attempt to unravel the mechanism whereby CAF-CD38 regulates endothelial tube formation, we examined the production of angiogenesis-related proteins in 3D cultures of MTAF CD38^{high} vs. MTAF CD38^{low}. Using a murine angiogenesis profiler array (see Material and Methods), we gauged on the expression of 53 angiogenesis-related proteins in lysates obtained from 3D cultured MTAFs. Equal protein loading, obtained from the lysates used for the above-mentioned array, aimed to compare 3D MTAF CD38^{high} vs. CD38^{low} secretion, was confirmed, via immunoblotting of the house keeping protein GAPDH (supplementary Fig. S3a, b). Quantification of the angiogenic profile expression revealed numerous differentially expressed proteins in MTAF CD38^{high} compared to MTAF CD38^{low} cells (Fig. 6a and supplementary Fig. S4). Results indicated significant reduced expression of pro-angiogenic proteins known to regulate: degradation and organization of ECM (MMP-9; $p < 0.01$), endothelial cell motility and hyper-permeability (VEGF-A ($p < 0.001$), HGF ($p < 0.05$), stabilization of pericytes (CXCL-12; ($p < 0.001$) and proliferation (FGF-2; $p < 0.001$) [28], in MTAF CD38^{low} compared to CD38^{high} (Fig. 6b–f). Transcription of the relevant genes *Mmp9*, *Vegfa*, *Hgf*, *Cxcl12* and *Fgf2* was gauged in mRNA collected from MTAF CD38^{high} vs. MTAF CD38^{low} cells cultured under 3D ECM producing conditions as before, via qRT-PCR. Results indicated a potential role for CD38 at the transcript levels for all tested genes (supplementary Fig. S5).

To assure that effects seen were induced by differences in CD38 expression and not due to exogenous TME cues, such as ECM, we also examined the levels of the five identified angiogenic transcripts in MTAF cells cultured under classic 2D conditions. Hence, we exposed the cells to no environmental stimuli [i.e., serum-free medium (SFM)] and compared results to effects imparted by the condition media collected from B16F10 cells, again, in the absence of ECM (i.e., 2D culturing). *Mmp9* and *Vegfa* mRNA levels were comparable in MTAF CD38^{high} vs. MTAF CD38^{low} cells grown in SFM, but significantly higher in MTAF CD38^{high} treated with B16F10 CM compared to MTAF CD38^{low} treated with B16F10 CM and MTAF CD38^{low} grown in SFM (Fig. 6g, h). Conversely, *Hgf*, *Cxcl12* and *Fgf2* mRNA levels were increased in MTAF CD38^{high} cells grown in SFM compared to CD38^{high} cells treated with CM, while levels in MTAF CD38^{low} were limited in MTAF CD38^{low} cells regardless of treatment (Fig. 6i–k). Taken together, these results suggest some intrinsic as well as selected extrinsic (CM and/or ECM) effects in the CAF CD38 regulation of pro-angiogenic transcription.

Discussion

It is well established that the TME plays a fundamental role in tumor progression. We showed previously that stromal CD38 inhibited melanoma outgrowth and reduced amount of CAFs and blood vessels, [10] indicating that the effect of stromal CD38 on melanoma is mediated via its effect on CAFs and blood vessels. Here we suggest that CD38 is a novel pro-melanoma regulator of CAF function; co-implantation of *Cd38*^{-/-} fibroblasts with B16F10 cells substantially reduced tumor growth and increased the lifespan of melanoma-bearing mice. We observed that CD38 increases fibroblastic migration towards tumor cells. Furthermore, CM collected from CD38-expressing fibroblasts enhanced tumor cell

migration and invasion, as well as endothelial vessel formation. Of note, the CD38-dependent tumor supporting effects of fibroblasts were evident in both genetically-engineered [17] primary fibroblasts and in an established CAF cell line [18]. Importantly, fibroblastic CD38 seemed to impart pro-tumor functions in a plethora of cells including melanoma and squamous-cell carcinoma tumor cells as well as in TME cells like endothelial cells.

Of note, in the co-injection experiments, the implanted fibroblasts overcome the tumor suppressive (*Cd38*^{-/-}) or tumor supporting effect (WT *Cd38*) imparted by the innate host microenvironment. This is probably due to the excess of the implanted fibroblasts over the innate host stromal cells, at least at early time after tumor cells injection. The co-injection experiments also show that co-injection of B16F10 cells and WT fibroblasts yielded similar tumor sizes in both WT and *Cd38*^{-/-} mice whereas the survival of the WT mice was worse than that of *Cd38*^{-/-} mice. This additional result implies that eventually the microenvironment of the host can too contribute to the overall survival of these mice. It is well established that CAFs regulate angiogenesis [5, 29]. Mechanistically, our results suggest that CD38 is a key driver of this CAF function, via regulation of the expression of key angiogenic factors like VEGF-A, FGF-2, CXCL-12, MMP-9 and HGF. Significant CD38-dependent differences in these factors were detected at both mRNA and protein levels. We observed that, at least in part, the underlying mechanism is regulated by CAF-generated ECMs, which have been also shown to control cytokine production (e.g., IL-8) [30]. In addition, CD38 can regulate intrinsic expression of angiogenic factors as suggested for VEGF-A in chronic lymphocytic leukemia cells [31].

Our previous results in melanoma mouse models, showed that targeting CD38 in the TME imparts therapeutic benefit [10]. Results in this study indicate that CD38 mediates pro-tumor functions in CAFs, yet this study cannot exclude the possibility that other CD38 expressing cells in the TME, such as macrophages [15] and T cells [32, 33], could contribute to the effects reported *in vivo*. Then again, our findings suggest that targeting CD38 may constitute a stroma normalizing therapeutic approach. The concept of CD38 targeting as an anti-tumor approach has been shown also in other systems. For example, targeting CD38 with the goal of improving anti-tumor immune therapy has been proposed [34]. Moreover, the anti-human CD38 antibody “daratumumab” has been approved for treating patients with multiple myeloma [35, 36]. Although anti-CD38 antibodies act mainly by killing the CD38-expressing tumor cells, it was shown that daratumumab can also modulate CD38 enzyme activity [37]. Hence, it will be interesting in future studies to test if anti-CD38 antibodies could inhibit CAF CD38-dependent pro-tumoral activities.

CD38 is also known for its ability to generate calcium mobilizing metabolites [12], which affect numerous cellular processes such as gene expression, metabolism, and chemotaxis. Further, it was reported that by regulating calcium levels, CD38 controls chemotaxis response in phagocytic cells [38, 39]. Whether similar mechanisms are involved in fibroblasts, remains to be determined. In addition, it will be interesting, in the future, to test whether CD38-generated metabolites could reinstitute the pro-tumoral functions upon *Cd38*^{-/-} fibroblasts. Similarly to CD38, the CD38 paralogue, CD157/BST1, has ADP-ribosyl cyclase and NAD glycohydrolase activities [14, 40]. It will also be interesting to

examine if it will too be capable of regulating/driving CAFs pro-tumoral functions. CD38 could also act by controlling levels of NAD⁺. In this way, CD38 could limit the activity of other NAD⁺-consuming enzymes, such as the histone deacetylase SIRT1, known to epigenetically control, amongst others, angiogenic gene expression [41]. Furthermore, through depleting NAD⁺ from the TME, CD38^{high} CAFs could reciprocally reprogram metabolic respiratory pathways in tumor cells, enabling a known anaerobically-active (i.e., highly tumorigenic) phenotype [42]. CD38 in fibroblasts may also act by inducing adenosine production via the CD38/CD203a/CD73 pathway [43]; in addition to CD38, CAFs can express PC1-/Cd203a [44] and CD73 [45]. Adenosine suppresses immune responses by its action on immune effector cells including fibroblasts, which have been shown to express the Adenosine 2B receptor (A2BR) [46]. Moreover, treatment of B16F10 melanoma-associated CAFs with an A2BR agonist, enhances CXCL12 and FGF2 expression in these cells [46].

Mouse CD38, the focus of the herein study, may differ from human CD38; a role for CD31 (PECAM-1) as a counter receptor of human CD38, but not mouse, has been proposed [11]. Since this study has employed mouse melanoma and skin fibroblastic cells, it could be of interest, if future studies could vet this studies' observations in a bona fide human melanoma TME.

In summary, we propose that CD38 regulates several key tumor-supporting effects in CAFs. Hence, fibroblastic CD38 targeting could be a valid potential therapeutic approach, which justifies additional studies. Fibroblastic dysfunction is associated with other fibrosis and inflammatory relevant diseases [4, 47]. Hence, the observed CAF CD38 effects may not be restricted to cancer.

Supplementary Material

Refer to Web version on PubMed Central for supplementary material.

Acknowledgments

We thank Prof. Neta Erez and Prof. Ronit Satchi-Fainaro for fruitful discussions and for providing the PDSC5 and B16F10 cells respectively. This work was supported in part by research grants from: Cancer Biology Research Center of TAU (to R. Stein). Support was also obtained from The Marvin and Concetta Greenberg Pancreatic Cancer Institute, Marianne DiNofrio Pancreatic Research Foundation, a philanthropic gift from Jeanne Leinen, Pennsylvania's DOH Health Research Formula Funds, the 5th AHEPA Cancer Research Foundation, the Worldwide Cancer Research Award, as well as NIH/NCI grants R21CA231252 (EC), R21CA228187 (EC), R01CA232256 (EC, JFB), and core grant CA06927 to support the Bio Sample Repository, Immune Monitoring, and Cell Culturing facilities at Fox Chase.

References

1. Bandarchi B, Jabbari CA, Vedadi A, Navab R. Molecular biology of normal melanocytes and melanoma cells. *J Clin Pathol*. 2013;66:644–648. [PubMed: 23526597]
2. Lacina L, Kodet O, Dvořánková B, Szabo P, Smetana K Jr., Ecology of melanoma cell. *Histol Histopathol*. 2018;33:247–254. [PubMed: 28849859]
3. Sahai E, Astsaturov I, Cukierman E, DeNardo DG, Egeblad M, Evans RM, et al. A framework for advancing our understanding of cancer-associated fibroblasts. *Nat Rev Cancer*. 2020.
4. Rybinski B, Franco-Barraza J, Cukierman E. The wound healing, chronic fibrosis, and cancer progression triad. *Physiological genomics*. 2014;46:223–244. [PubMed: 24520152]

5. Zhou L, Yang K, Andl T, Wickett RR, Zhang Y. Perspective of Targeting Cancer-Associated Fibroblasts in Melanoma. *Journal of Cancer*. 2015;6:717–726. [PubMed: 26185533]
6. Sahai E, Astsaturov I, Cukierman E, DeNardo DG, Egeblad M, Evans RM, et al. A framework for advancing our understanding of cancer-associated fibroblasts. *Nat Rev Cancer*. 2020;20:174–186. [PubMed: 31980749]
7. Franco-Barraza J, Francescone R, Luong T, Shah N, Madhani R, Cukierman G, et al. Matrix-regulated integrin $\alpha 5 \beta 1$ maintains $\alpha 5 \beta 1$ -dependent desmoplastic traits prognostic of neoplastic recurrence. *eLife*. 2017;6.
8. Gupta V, Bassi DE, Simons JD, Devarajan K, Al-Saleem T, Uzzo RG, et al. Elevated expression of stromal palladin predicts poor clinical outcome in renal cell carcinoma. *PLoS ONE*. 2011;6:e21494. [PubMed: 21738681]
9. Goetz JG, Minguet S, Navarro-Lerida I, R JLL, Samaniego R, Calvo E, et al. Biomechanical remodeling of the microenvironment by stromal caveolin-1 favors tumor invasion and metastasis. *Cell*. 2011;146:148–163. [PubMed: 21729786]
10. Ben Baruch B, Blacher E, Mantsur E, Schwartz H, Vaknine H, Erez N, et al. Stromal CD38 regulates outgrowth of primary melanoma and generation of spontaneous metastasis. *Oncotarget*. 2018;9:31797–31811. [PubMed: 30159123]
11. Malavasi F, Deaglio S, Funaro A, Ferrero E, Horenstein AL, Ortolan E, et al. Evolution and function of the ADP ribosyl cyclase/CD38 gene family in physiology and pathology. *Physiol Rev*. 2008;88:841–886. [PubMed: 18626062]
12. Chini EN, Chini CCS, Espindola Netto JM, de Oliveira GC, van Schooten W. The Pharmacology of CD38/NADase: An Emerging Target in Cancer and Diseases of Aging. *Trends Pharmacol Sci*. 2018;39:424–436. [PubMed: 29482842]
13. Lund FE. Signaling properties of CD38 in the mouse immune system: enzyme-dependent and -independent roles in immunity. *Mol Med*. 2006;12:328–333. [PubMed: 17380200]
14. Quarona V, Zaccarello G, Chillemi A, Brunetti E, Singh VK, Ferrero E, et al. CD38 and CD157: a long journey from activation markers to multifunctional molecules. *Cytometry B Clin Cytom*. 2013;84:207–217. [PubMed: 23576305]
15. Levy A, Blacher E, Vaknine H, Lund FE, Stein R, Mayo L. CD38 deficiency in the tumor microenvironment attenuates glioma progression and modulates features of tumor-associated microglia/macrophages. *Neuro Oncol*. 2012;14:1037–1049. [PubMed: 22700727]
16. Blacher E, Ben Baruch B, Levy A, Geva N, Green KD, Garneau-Tsodikova S, et al. Inhibition of glioma progression by a newly discovered CD38 inhibitor. *Int J Cancer*. 2015;136:1422–1433. [PubMed: 25053177]
17. Cockayne DA, Muchamuel T, Grimaldi JC, Muller-Steffner H, Randall TD, Lund FE, et al. Mice deficient for the ecto-nicotinamide adenine dinucleotide glycohydrolase CD38 exhibit altered humoral immune responses. *Blood*. 1998;92:1324–1333. [PubMed: 9694721]
18. Amatangelo MD, Bassi DE, Klein-Szanto AJ, Cukierman E. Stroma-derived three-dimensional matrices are necessary and sufficient to promote desmoplastic differentiation of normal fibroblasts. *Am J Pathol*. 2005;167:475–488. [PubMed: 16049333]
19. Cukierman E, Pankov R, Stevens DR, Yamada KM. Taking cell-matrix adhesions to the third dimension. *Science*. 2001;294:1708–1712. [PubMed: 11721053]
20. Arbeit JM, Munger K, Howley PM, Hanahan D. Progressive squamous epithelial neoplasia in K14-human papillomavirus type 16 transgenic mice. *J Virol*. 1994;68:4358–4368. [PubMed: 7515971]
21. Franco-Barraza J, Raghavan KS, Luong T, Cukierman E. Engineering clinically-relevant human fibroblastic cell-derived extracellular matrices. *Cell-derived Matrices Methods in Cell Biology*: Elsevier, 2020.
22. Arnaoutova I, Kleinman HK. In vitro angiogenesis: endothelial cell tube formation on gelled basement membrane extract. *Nature protocols*. 2010;5:628–635. [PubMed: 20224563]
23. Kaur A, Ecker BL, Douglass SM, Kugel CH 3rd, Webster MR, Almeida FV, et al. Remodeling of the Collagen Matrix in Aging Skin Promotes Melanoma Metastasis and Affects Immune Cell Motility. *Cancer Discov*. 2019;9:64–81.
24. Liang CC, Park AY, Guan JL. In vitro scratch assay: a convenient and inexpensive method for analysis of cell migration in vitro. *Nat Protoc*. 2007;2:329–333. [PubMed: 17406593]

25. Chiang SP, Cabrera RM, Segall JE. Tumor cell intravasation. *Am J Physiol Cell Physiol*. 2016;311:C1–C14. [PubMed: 27076614]
26. Wang FT, Sun W, Zhang JT, Fan YZ. Cancer-associated fibroblast regulation of tumor neo-angiogenesis as a therapeutic target in cancer. *Oncology letters*. 2019;17:3055–3065. [PubMed: 30867734]
27. Erdogan B, Webb DJ. Cancer-associated fibroblasts modulate growth factor signaling and extracellular matrix remodeling to regulate tumor metastasis. *Biochemical Society transactions*. 2017;45:229–236. [PubMed: 28202677]
28. Carmeliet P, Jain RK. Angiogenesis in cancer and other diseases. *Nature*. 2000;407:249–257. [PubMed: 11001068]
29. Newman AC, Nakatsu MN, Chou W, Gershon PD, Hughes CC. The requirement for fibroblasts in angiogenesis: fibroblast-derived matrix proteins are essential for endothelial cell lumen formation. *Mol Biol Cell*. 2011;22:3791–3800. [PubMed: 21865599]
30. Paulitti A, Andreuzzi E, Bizzotto D, Pellicani R, Tarticchio G, Marastoni S, et al. The ablation of the matricellular protein EMILIN2 causes defective vascularization due to impaired EGFR-dependent IL-8 production affecting tumor growth. *Oncogene*. 2018;37:3399–3414. [PubMed: 29483644]
31. Molica S, Cutrona G, Vitelli G, Mirabelli R, Molica M, Digiesi G, et al. Markers of increased angiogenesis and their correlation with biological parameters identifying high-risk patients in early B-cell chronic lymphocytic leukemia. *Leukemia research*. 2007;31:1575–1578. [PubMed: 17485110]
32. Chatterjee S, Daenthansanmak A, Chakraborty P, Wyatt MW, Dhar P, Selvam SP, et al. CD38-NAD(+)Axis Regulates Immunotherapeutic Anti-Tumor T Cell Response. *Cell metabolism*. 2018;27:85–100 e108. [PubMed: 29129787]
33. Morandi F, Morandi B, Horenstein AL, Chillemi A, Quarona V, Zaccarello G, et al. A non-canonical adenosinergic pathway led by CD38 in human melanoma cells induces suppression of T cell proliferation. *Oncotarget*. 2015;6:25602–25618. [PubMed: 26329660]
34. Chen L, Diao L, Yang Y, Yi X, Rodriguez BL, Li Y, et al. CD38-Mediated Immunosuppression as a Mechanism of Tumor Cell Escape from PD-1/PD-L1 Blockade. *Cancer Discov*. 2018;8:1156–1175.
35. Lokhorst HM, Plesner T, Laubach JP, Nahi H, Gimsing P, Hansson M, et al. Targeting CD38 with Daratumumab Monotherapy in Multiple Myeloma. *N Engl J Med*. 2015;373:1207–1219. [PubMed: 26308596]
36. van de Donk N. Reprint of “Immunomodulatory effects of CD38-targeting antibodies”. *Immunol Lett*. 2019;205:71–77. [PubMed: 30826127]
37. van de Donk NW, Janmaat ML, Mutis T, Lammerts van Bueren JJ, Ahmadi T, Sasser AK, et al. Monoclonal antibodies targeting CD38 in hematological malignancies and beyond. *Immunological reviews*. 2016;270:95–112. [PubMed: 26864107]
38. Partida-Sanchez S, Iribarren P, Moreno-Garcia ME, Gao JL, Murphy PM, Oppenheimer N, et al. Chemotaxis and calcium responses of phagocytes to formyl peptide receptor ligands is differentially regulated by cyclic ADP ribose. *J Immunol*. 2004;172:1896–1906. [PubMed: 14734775]
39. Partida-Sanchez S, Cockayne DA, Monard S, Jacobson EL, Oppenheimer N, Garvy B, et al. Cyclic ADP-ribose production by CD38 regulates intracellular calcium release, extracellular calcium influx and chemotaxis in neutrophils and is required for bacterial clearance in vivo. *Nat Med*. 2001;7:1209–1216. [PubMed: 11689885]
40. Ferrero E, Lo Buono N, Morone S, Parrotta R, Mancini C, Brusco A, et al. Human canonical CD157/Bst1 is an alternatively spliced isoform masking a previously unidentified primate-specific exon included in a novel transcript. *Sci Rep*. 2017;7:15923. [PubMed: 29162908]
41. Potente M, Dimmeler S. Emerging roles of SIRT1 in vascular endothelial homeostasis. *Cell Cycle*. 2008;7:2117–2122. [PubMed: 18641460]
42. Chiarugi A, Dolle C, Felici R, Ziegler M. The NAD metabolome--a key determinant of cancer cell biology. *Nat Rev Cancer*. 2012;12:741–752. [PubMed: 23018234]

43. Horenstein AL, Bracci C, Morandi F, Malavasi F. CD38 in Adenosinergic Pathways and Metabolic Re-programming in Human Multiple Myeloma Cells: In-tandem Insights From Basic Science to Therapy. *Frontiers in immunology*. 2019;10:760. [PubMed: 31068926]
44. Reaven GM. Banting lecture 1988. Role of insulin resistance in human disease. *Diabetes*. 1988;37:1595–1607. [PubMed: 3056758]
45. Aoki M, Koga K, Miyazaki M, Hamasaki M, Koshikawa N, Oyama M, et al. CD73 complexes with emmprin to regulate MMP-2 production from co-cultured sarcoma cells and fibroblasts. *BMC cancer*. 2019;19:912. [PubMed: 31510956]
46. Sorrentino C, Miele L, Porta A, Pinto A, Morello S. Activation of the A2B adenosine receptor in B16 melanomas induces CXCL12 expression in FAP-positive tumor stromal cells, enhancing tumor progression. *Oncotarget*. 2016;7:64274–64288. [PubMed: 27590504]
47. McAnulty RJ. Fibroblasts and myofibroblasts: their source, function and role in disease. *Int J Biochem Cell Biol*. 2007;39:666–671. [PubMed: 17196874]

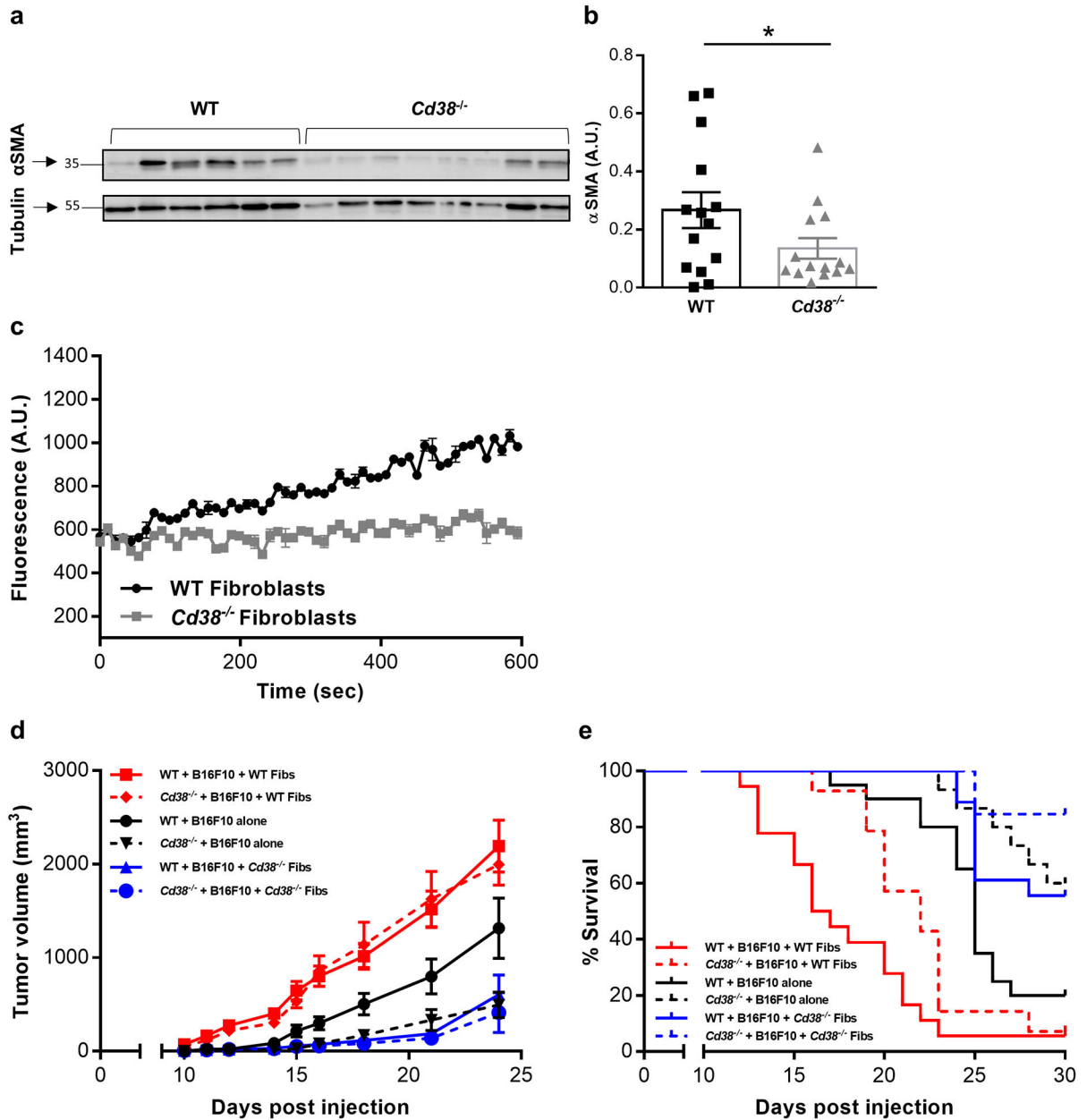


Fig. 1. Fibroblastic CD38 regulates melanoma outgrowth.

a-b Immunoblot analysis of α -SMA expression in tumors grown in *Cd38^{-/-}* vs. WT mice.

Twenty-eight days post tumor implantation, protein extracts were prepared from the excised tumors and α -SMA protein levels were determined. **a** Representative immunoblot probed for α -SMA and β -tubulin; each lane represents a different tumor. **b** Quantification of α -SMA levels. α -SMA level is denoted as arbitrary units (A.U.) representative of signal-intensity values normalized to β -tubulin. Error bars represent mean \pm S.E.M (Student's *t* test, *n* = 14 samples for each group). **c** CD38 enzyme activity in primary WT and *Cd38^{-/-}* fibroblasts. Results shown are from one representative, out of two, experiments conducted independently. **d-e** Effect of WT and *Cd38^{-/-}* fibroblasts on B16F10 melanoma outgrowth. WT or *Cd38^{-/-}* mice were injected (subcutaneously) with B16F10 cells alone or together

with WT vs. *Cd38*^{-/-} fibroblasts (Fibs). Tumor volume was measured at the indicated time points. **d** Quantification of tumor volume. Results are from 3 independent experiments, values are presented as mean ± S.E.M. (n = 19, 15 or 18, 13, or 19, 13 mice for B16F10 alone, B16F10 + WT or B16F10 + *Cd38*^{-/-} fibroblasts injected to WT or *Cd38*^{-/-} mice, respectively). Two-way ANOVA with repeated measures followed by Tukey post hoc test, revealed significant effect for: time per treatment ($p < 0.0001$) within subjects, and for treatment between subjects ($p < 0.0001$). **e** Kaplan-Meier survival curve. Survival of WT mice injected with B16F10 cells was significantly (log-rank test; $p < 0.0001$) higher when co-injected with *Cd38*^{-/-} fibroblasts than with WT fibroblasts. Similarly, survival of *Cd38*^{-/-} mice, injected with B16F10 cells, was significantly higher (log-rank test; $p < 0.0001$) when co-injected with *Cd38*^{-/-} fibroblasts compared to WT.

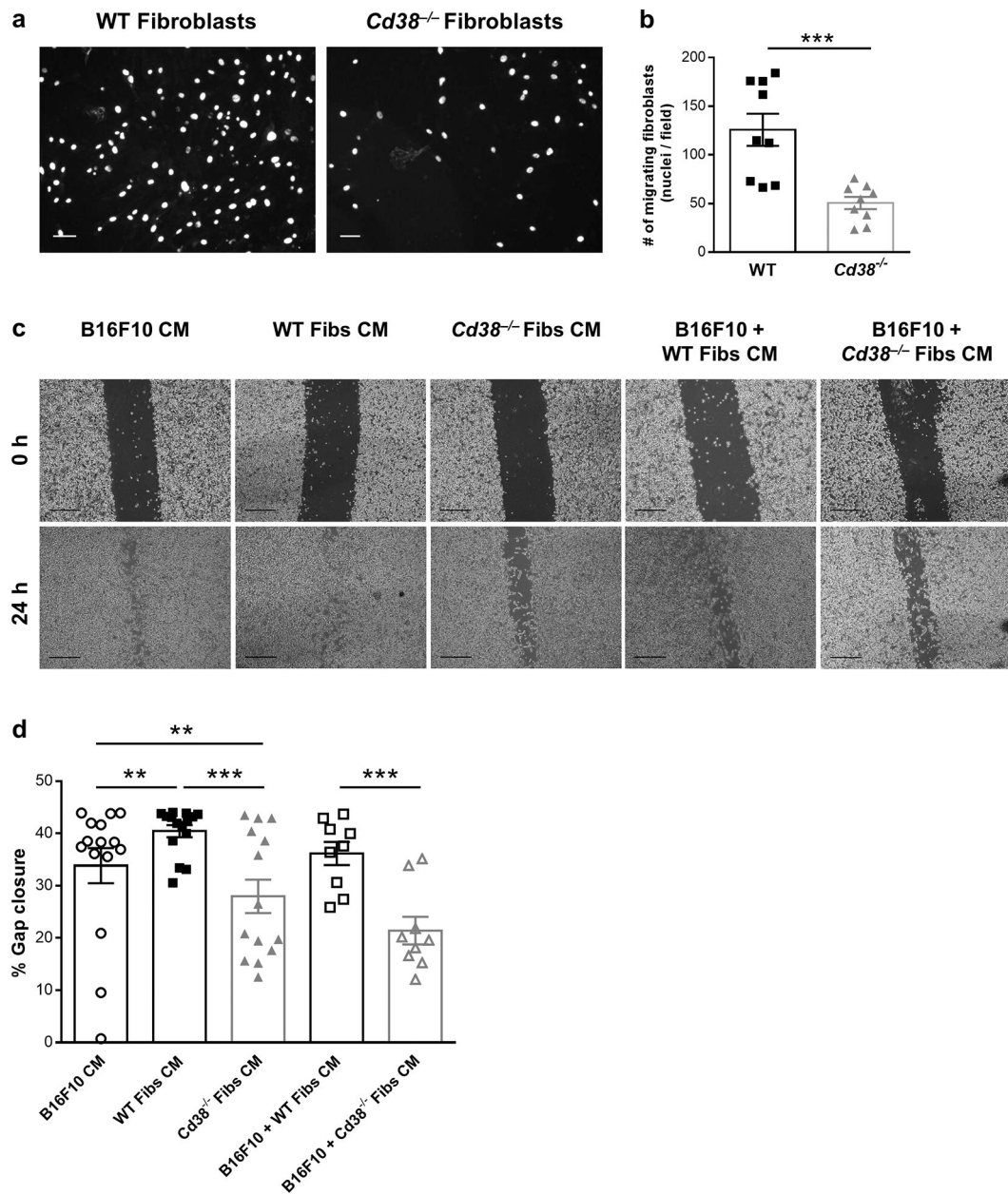


Figure 2. CD38 in fibroblasts regulates migration of fibroblasts and B16F10 melanoma cells.
a-b Loss of CD38 in fibroblasts inhibits fibroblasts' migratory response towards melanoma cells. WT or *Cd38*^{-/-} fibroblasts were plated on the upper face of transwell inserts and B16F10 cells in the lower chamber. The number of transmigrated fibroblasts after 24 h was determined as described in Materials and Methods. **a** Representative images of fluorescent (Hoechst)-labeled nuclei from transmigrated fibroblasts. Scale bar = 100 μ m. **b** Quantification of transmigration results. The results shown are number of nuclei in a captured field. Error bars represent mean \pm S.E.M (Student's *t* test, $p = 0.0002$, $n = 3$). **c-d** CD38 regulates the effect of fibroblast's CM on B16F10 migration. CM were prepared from B16F10 cells (B16F19 CM), WT fibroblasts (WT Fibs CM), *Cd38*^{-/-} fibroblasts (*Cd38*^{-/-} fibs CM), co-cultures of B16F10 together with WT fibroblasts (B16F10 + WT Fibs CM) or

with *Cd38*^{-/-} fibroblasts (B16F10 + *Cd38*^{-/-} Fibs CM). A scratch wound was inflicted on B16F10 cells monolayer supplemented with the indicated CM. The resulting gap width was imaged immediately after (0 h) and after 24 h. **c** Representative images of the scratch areas at 0 h and 24 h. Scale bar = 500 μ m. **d** Quantification of gap closure. The results shown are expressed as the percentage of gap closure after 24 h from t = 0 h. Error bars represent mean \pm S.E.M. Two-way ANOVA ($p < 0.001$) with Bonferroni's multiple comparisons test was performed to determine statistical significance (n = 5).

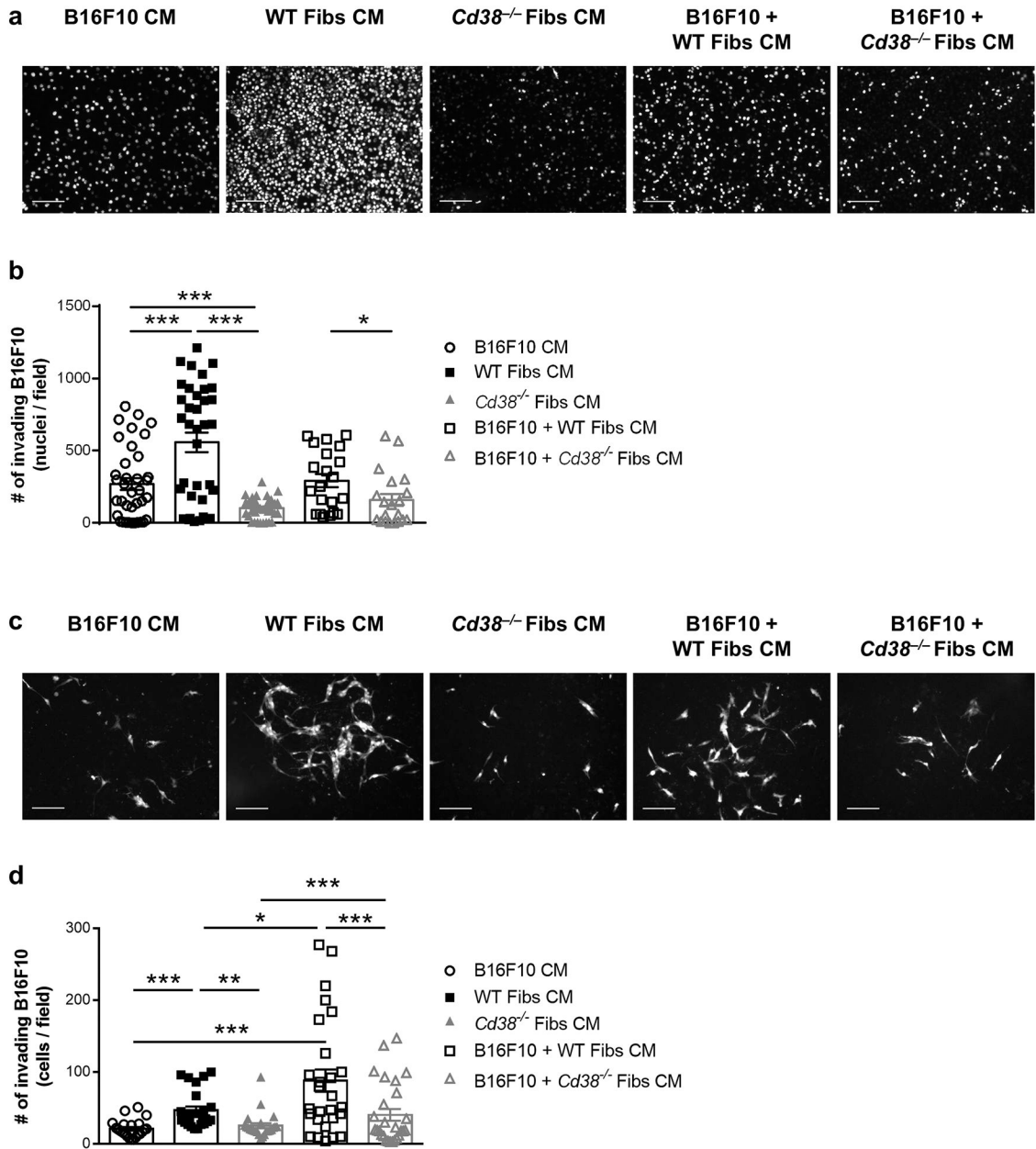


Figure 3. CD38 regulates the effect of fibroblast’s CM on B16F10 invasion.

a-b Invasion across basement membrane preparation (Cultrex). B16F10 cells were seeded on the upper face of Cultrex-coated transwell inserts. Indicated CM were added to the lower chambers. After 24 h invaded cells were detected and images captured and analyzed as described in Materials and Methods. **a** Representative monochromatic images of Invading B16F10 cells identified by their fluorescent nuclei. Scale bar = 500 μ m. **b** Quantification of invasion through Cultrex. Results shown represent the number of fluorescent nuclei per field. Error bars represent mean \pm S.E.M. Two-way ANOVA with Bonferroni’s multiple comparisons test was performed to determine statistical significance. ($n = 6$). **c-d** Invasion across MECs monolayer. Invading mCherry B16F10 cells were detected after 24 h. **c** Representative monochromatic images of invading B16F10 cells. Scale bar = 500 μ m. **d**

Quantification of the invasion across MECs results. Graph represents number of cells per field. Error bars represent mean \pm S.E.M. Two-way ANOVA with Bonferroni's multiple comparisons test was performed to determine statistical significance ($n = 4$).

Author Manuscript

Author Manuscript

Author Manuscript

Author Manuscript

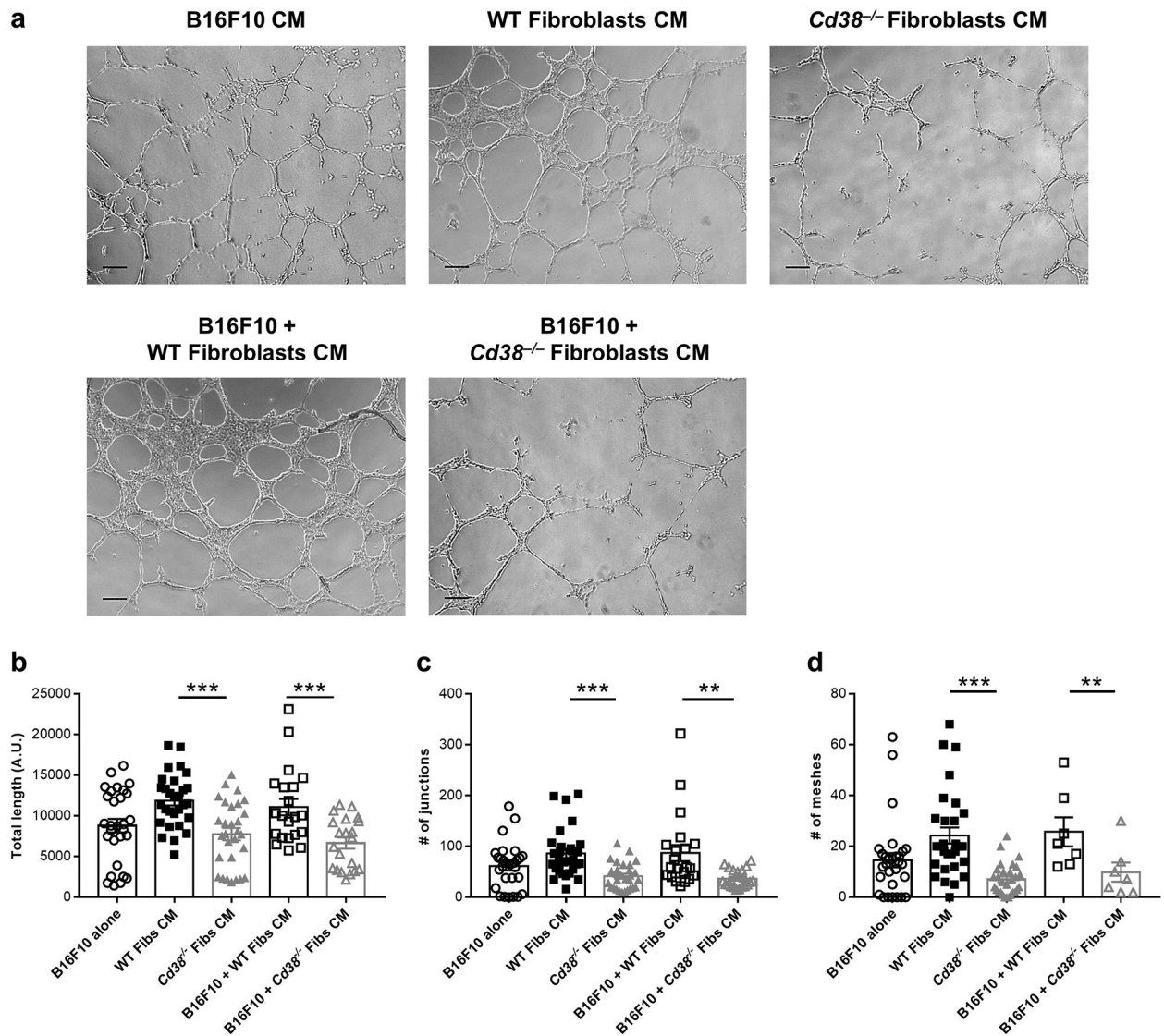


Figure 4. CD38 regulates the effect of fibroblast's CM on MECs tube formation.

MECs mixed with the indicated CM were seeded on Cultrex-coated 24-well plates. Phase contrast images were captured after 10 h of culturing. **a** Representative images (scale bar = 200 μ m). **b** Quantification of total vessels length, **c** number of junctions (branching point of 3 tubes), and **d** number of meshes (closed segments), per field was performed using ImageJ and Angiogenesis Analyzer plugin. Error bars represent mean \pm S.E.M. Two-way ANOVA with Bonferroni's multiple comparisons test was performed to determine statistical significance ($n = 4$).

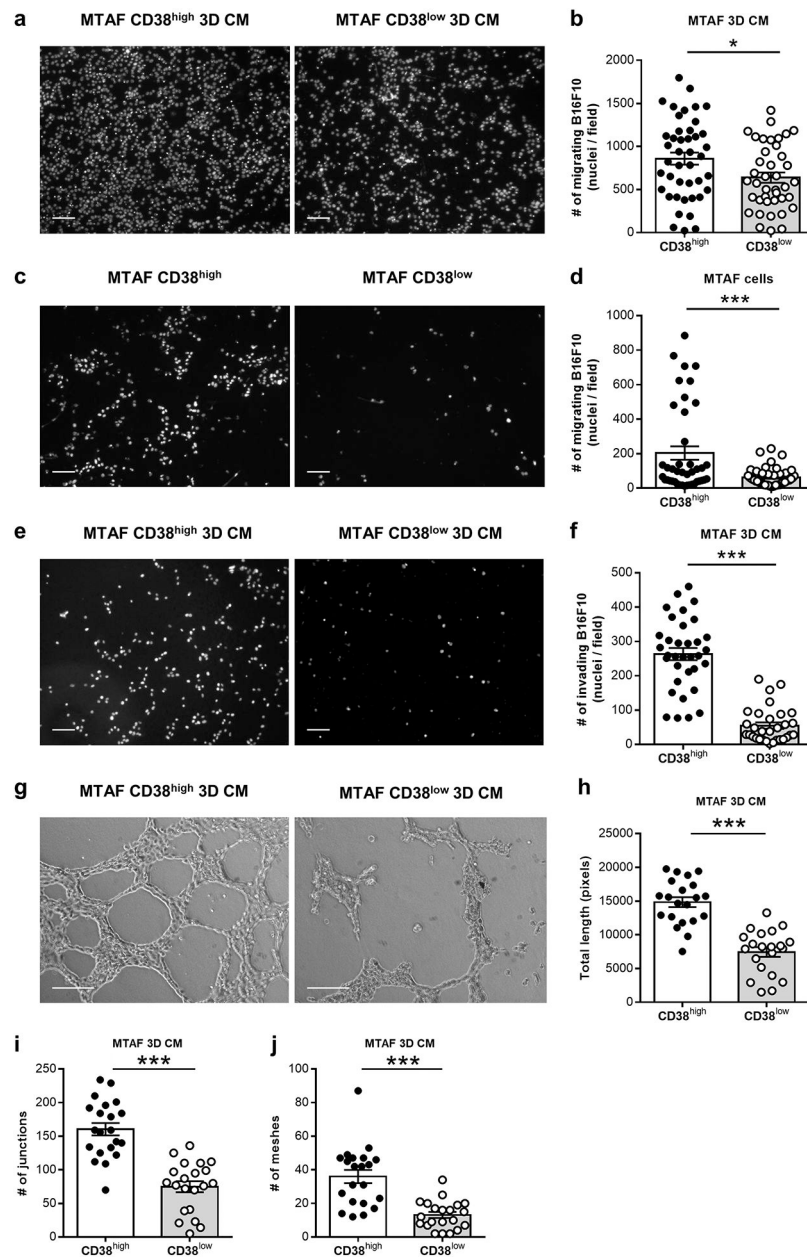


Figure 5. CD38 in MTAF cells regulates B16F10 cells migration and invasion and endothelial tube formation.

a-b Transmigration of B16F10 cells in the presence of CM from the indicated MTAF populations in 3D culture. After 24 h the amount of migrated cells was determined. **a** Representative images of migrated B16F10 cells (fluorescent nuclei). Scale bar = 100 μ m. **b** Quantification of the migration results. The results shown represent the number of nuclei in a captured field. Error bars represent mean \pm S.E.M (Student's *t* test, *n* = 3). **c-d** The effect of MTAF CD38^{high} and MTAF CD38^{low} cells on B16F10 cells migration. MTAF cells were plated in the lower chamber and B16F10 cells in the upper chamber. B16F10 transwell migration was assessed after 24 h. **c** Representative images of migrated cells (fluorescent nuclei). Scale bar = 100 μ m. **d** Quantification of the migration results. The results shown are

number of nuclei in a captured field. Error bars represents mean \pm S.E.M (Student's *t* test, *n* = 3). **e-f** The effect of MTAF's 3D CM on B16F10 cells invasion. **e** Representative images of B16F10 cells (fluorescent nuclei). Scale bar = 100 μ m. **f** Quantification of the invasion. The results shown are number of nuclei in a captured field. Error bars represent mean \pm S.E.M (Student's *t* test *n* = 3). **g-j** The effect of MTAF's 3D CM on MECs tube formation. **g** Representative phase contrast images of the vessels network after 8 h (scale bar = 200 μ m). Quantification of total vessels length **h**, number of junctions **i**, and meshes **j**. Error bars represent mean \pm S.E.M. (Student's *t* test, *n* = 4).

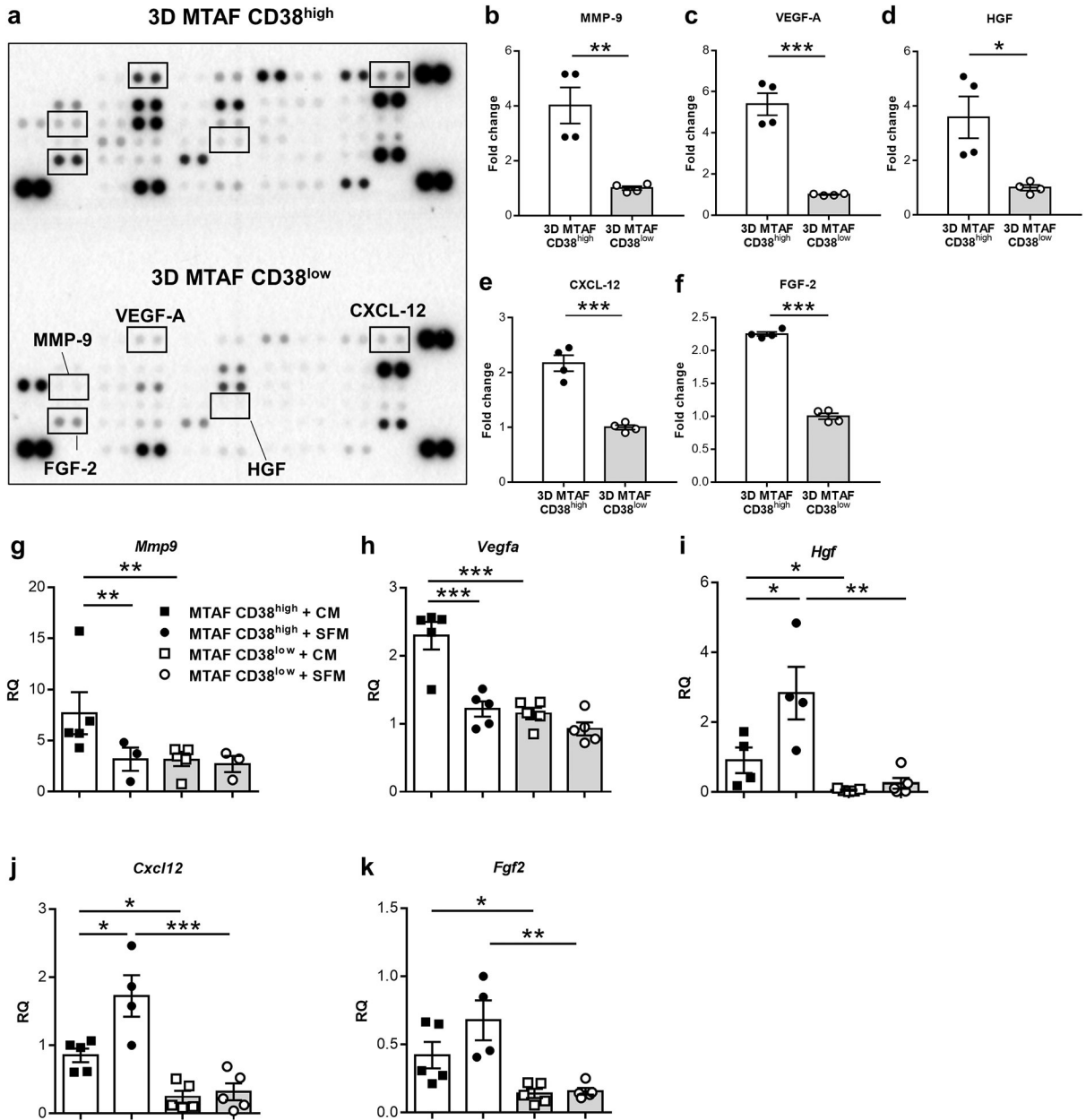


Figure 6. CD38-dependent differential expression of angiogenic proteins and genes in MTAF cells.

a-f CD38-dependent regulation of angiogenesis-related proteins expression in MTAF cells grown in 3D cultures CAFs. The expression of angiogenesis-related proteins was analyzed using murine angiogenesis profiler array in two independent experiments. **a** Image of a representative membrane analyzed showing the expression pattern of angiogenesis-related proteins. **b-f** Expression profiles for MMP-9 **b**, VEGF-A **c**, HGF **d**, CXCL-12 **e** and FGF-2 **f** proteins. The pixel density of each dot in the array was quantified using ImageJ. Results are presented as fold change relative to the corresponding protein in MTAF CD38^{low} cells. Error bars represent mean \pm S.E.M. (Student's *t* test; results shown are from 2 independent experiments). **g-k** mRNA levels of *Mmp9* **g**, *Vegfa* **h**, *Hgf* **i**, *Cxcl12* **j** and *Fgf2* **k** from

MTAF cultured in 2D conditions, treated with either serum free medium (SFM) or with B16F10 CM (CM) for 48 h. mRNA levels were determined by qRT-PCR. Results are presented as RQ from 5 independent experiments. Error bars represent mean \pm S.E.M. Two-way ANOVA with Bonferroni's multiple comparisons test was performed to determine statistical significance.

Author Manuscript

Author Manuscript

Author Manuscript

Author Manuscript